Received: 5 December 2022 | Revised: 23 April 2023 | Accepted: 11 May 2023

DOI: 10.1111/gcb.16806

Global Change Biology WILEY

RESEARCH ARTICLE

# $CO_2$ fertilization contributed more than half of the observed forest biomass increase in northern extra-tropical land

Yue He[1] | Yongwen Liu[2] | Lingjie Lei[1] | César Terrer[3] | Chris Huntingford[4] | Josep Peñuelas[5,6] | Hao Xu[1] | Shilong Piao[1,2]

[1]Sino-French Institute for Earth System Science, College of Urban and Environmental Sciences, Peking University, Beijing, China

[2]State Key Laboratory of Earth System and Environmental Resources of the Tibetan Plateau (TPESER), Institute of Tibetan Plateau Research, Chinese Academy of Sciences, Beijing, China

[3]Department of Civil and Environmental Engineering, Massachusetts Institute of Technology, Cambridge, Massachusetts, USA

[4]UK Centre for Ecology and Hydrology, Wallingford, UK

[5]CREAF, Cerdanyola del Valles, Barcelona, Spain

[6]CSIC, Global Ecology Unit CREAF-CSIC-UAB, Barcelona, Spain

**Correspondence**
Yongwen Liu, State Key Laboratory of Earth System and Environmental Resources of the Tibetan Plateau (TPESER), Institute of Tibetan Plateau Research, Chinese Academy of Sciences, Beijing 100101, China.
Email: liuyongwen@itpcas.ac.cn

Shilong Piao, Sino-French Institute for Earth System Science, College of Urban and Environmental Sciences, Peking University, Beijing 100871, China.
Email: slpiao@pku.edu.cn

**Funding information**
National Natural Science Foundation of China, Grant/Award Number: 41988101 and 42122005; Youth Innovation Promotion Association of the Chinese Academy of Sciences, Grant/Award Number: 2019074

## Abstract

The existence of a large-biomass carbon (C) sink in Northern Hemisphere extra-tropical ecosystems (NHee) is well-established, but the relative contribution of different potential drivers remains highly uncertain. Here we isolated the historical role of carbon dioxide ($CO_2$) fertilization by integrating estimates from 24 $CO_2$-enrichment experiments, an ensemble of 10 dynamic global vegetation models (DGVMs) and two observation-based biomass datasets. Application of the emergent constraint technique revealed that DGVMs underestimated the historical response of plant biomass to increasing [$CO_2$] in forests ($\beta^{Mod}_{Forest}$) but overestimated the response in grasslands ($\beta^{Mod}_{Grass}$) since the 1850s. Combining the constrained $\beta^{Mod}_{Forest}$ ($0.86 \pm 0.28$ kg C $m^{-2}$ [100 ppm]$^{-1}$) with observed forest biomass changes derived from inventories and satellites, we identified that $CO_2$ fertilization alone accounted for more than half ($54 \pm 18\%$ and $64 \pm 21\%$, respectively) of the increase in biomass C storage since the 1990s. Our results indicate that $CO_2$ fertilization dominated the forest biomass C sink over the past decades, and provide an essential step toward better understanding the key role of forests in land-based policies for mitigating climate change.

**KEYWORDS**
carbon cycling, $CO_2$ fertilization, $CO_2$-enrichment experiments, dynamic global vegetation models, emergent constrain

## 1 | INTRODUCTION

Terrestrial ecosystems have absorbed approximately 32% of the anthropogenic emissions of carbon dioxide ($CO_2$) since preindustrial times, broadly taken as the years 1850 to the present day (Friedlingstein et al., 2020). Such absorption has appreciably slowed the rate of global warming (Ballantyne et al., 2012; Schimel et al., 2015; Shevliakova et al., 2013). The substantial increase in the

  

amount of biomass carbon (C) stored in Northern Hemisphere extratropical ecosystems (NHee) is thought to be an important part of the overall enhanced global terrestrial C sink (Liu et al., 2015; Pan et al., 2011; Tagesson et al., 2020; Xu et al., 2021). Such an increase in biomass is simultaneously regulated by multiple covarying factors, such as the $CO_2$ fertilization effect (CFE), climate change, nitrogen (N) deposition and land-use change, complicating the quantification of their individual effects (Fernández-Martínez et al., 2019; Peylin et al., 2013; Reich et al., 2020; Sitch et al., 2015). Previous studies have generally suggested that $CO_2$ fertilization drove the primary gain in stores of biomass C (Huntzinger et al., 2017; Piao et al., 2013; Schimel et al., 2015; Walker et al., 2021; Wenzel et al., 2016), but the direct impacts of climate change could ultimately suppress such gains in the future (Jiao et al., 2021; Peñuelas et al., 2017; Piao et al., 2020; Yuan et al., 2019), while limited N availability may eventually lower the ability to "draw down" atmospheric $CO_2$ concentrations ($[CO_2]$; Norby et al., 2010; Terrer et al., 2019; Zaehle et al., 2015). Isolating and accurately quantifying the magnitude of $CO_2$ fertilization and its contribution is accordingly essential, with implications for the formulation and implementation of land-based mitigation strategies that may maximize the offset of $CO_2$ emissions.

Considerable efforts have been made in recent decades to improve our knowledge of the CFE on the terrestrial C cycle, in particular by conducting $CO_2$-enrichment experiments, many, but not all, of which report that elevated $[CO_2]$ has stimulated plant growth and biomass C sequestration (McCarthy et al., 2010; Terrer et al., 2019; Walker et al., 2021). Site-scale measurements can provide critical local information on CFE, but they have limited ability to represent geographically extensive changes or long-term results due to their relative scarcity and short duration (~5 years on average; Terrer et al., 2021). As an alternative, dynamic global vegetation models (DGVMs) can provide complete geographical coverage and be configured to isolate and quantify long-term CFE around the globe, but require accurate parameterization. DGVMs collectively agree that CFE is the dominant cause of the increase in biomass, but large inter-DGVMs exist, causing uncertainty in their projections (Haverd et al., 2020; Schimel et al., 2015). For example, an ensemble of DGVMs from the Trends in Net Land Atmosphere Carbon Exchanges project version 9 (TRENDYv9) showed that the simulated increase in CFE-induced plant biomass in NHee during 1850–2019 varied from 11.25 Pg C in the LPX-Bern model to 54.15 Pg C in the CABLE-POP model. Observations from site-based $CO_2$-enrichment experiments and the outputs from DGVMs are not directly comparable, so a newly emerged mathematical approach, the so-called emergent constraint (Cox et al., 2013; Eyring et al., 2019; He et al., 2020; Lian et al., 2018; see Section 2), can be used to reconcile the spatial–temporal mismatch between them, for better understanding the historical effect of $CO_2$ fertilization on plant biomass.

Our overall aim is to quantify the specific role of $CO_2$ fertilization, based on both models and observations, in driving the biomass C sequestration in NHee ecosystems. We first used emergent constraint approach to derive the response of plant biomass to increasing $[CO_2]$ (parameter $\beta$) in NHee from 1850 to 2019, resolving into all total vegetation, or forest/grassland only (see Section 2). Then, for the shorter period of 1990–2019, we presented much more specific information, with the fertilization effect disaggregated into further biome classifications and for six key different countries/regions in NHee. Using the inferred constraints in combination with observed forest biomass changes reported previously (Pan et al., 2011; Xu et al., 2021), we thus estimated the contribution of CFE for whole NHee and each of the six major countries/regions since the 1990s. Our database is comprised of 41 field observations collected at 24 $CO_2$-enrichment experiments in forest and grassland systems (Table S1; Figure S1), together with the outputs of the 10 DGVMs from the TRENDY ensemble. Since $CO_2$-enrichment experiments and DGVMs have very different settings for $[CO_2]$ increases ($\Delta CO_2$), there are two important transformations to be addressed to align the models with the data before emergent constraint (Figure 1). First, to simulate the step increase in $[CO_2]$ common in $CO_2$-enrichment experiments, we calibrated the DGVM outputs, originally simulating a gradual increase in $[CO_2]$, over the grid cells corresponding to the experimental sites using a two-box model (Liu et al., 2019). Second, to match the magnitude of $\Delta CO_2$ at historical levels (e.g., from 286.46 to 409.39 ppm during 1850–2019), we converted the experimental CFE, originally conducted at future $[CO_2]$ levels (e.g., from ~380 to ~610 ppm) using a theoretical model of photosynthesis (P-model; see Section 2).

## 2 | MATERIALS AND METHODS

### 2.1 | Study region

Our study region was restricted to NHee, defined as the areas between 23°N and 90°N including a southern part of China below 23°N for integrity (Figure S1). We used the Collection-5 MODIS land-cover product (MCD12C1) with the classification scheme of the International Geosphere-Biosphere Programme at a resolution of 0.05° for 2001. This NHee vegetation map was first aggregated to a resolution of 0.5° by dominant types of land cover, and the 17 land-cover types were then reclassified into four classes by biome: temperate forest (forests <55°N), boreal forest (forests >55°N), grassland, and other biomes. We divided the NHee forest areas into six major countries/regions to further determine the CFE at a regional scale following the region map in Pan et al. (2011): Canada, northern Europe, Russia, the United States, temperate Europe, and China. Note that boreal forests are mainly distributed in Canada, northern Europe, and Russia and that temperate forests are mainly distributed in the United States, temperate Europe, and China.

### 2.2 | Observed CFE on plant biomass from $CO_2$-enrichment experiments

We collected data on the effect of $CO_2$ fertilization on plant biomass in forest and grassland ecosystems by assembling the $CO_2$-enrichment

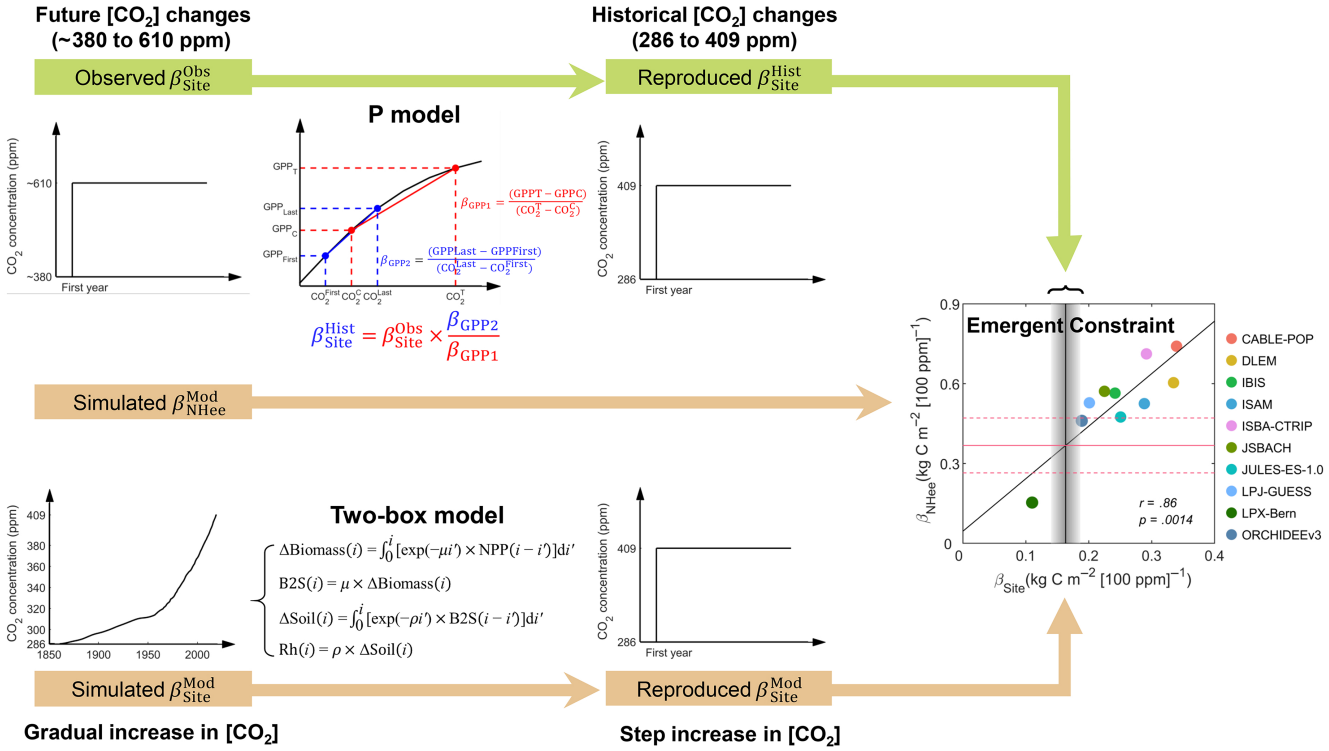


FIGURE 1 Schematic overview of the methodology used for the transformation of $[CO_2]$-related settings between model and data. Green arrows show the methodological steps to convert observed site-scale $CO_2$ fertilization effect (CFE) on plant biomass at future $[CO_2]$ levels ($\beta^{Obs}_{Site}$) to CFE at historical $[CO_2]$ levels ($\beta^{Hist}_{Site}$) for the $CO_2$ experiments. Brown arrows represent the methodological steps to convert simulated site-scale CFE on plant biomass with a gradual increase in $[CO_2]$ to a step increase in $[CO_2]$ ($\beta^{Mod}_{Site}$), and this value together with the simulated Northern Hemisphere extra-tropical ecosystems (NHee)-scale CFE ($\beta^{Mod}_{NHee}$) were then used to build a linear relationship across the dynamic global vegetation models for further emergent constraint. All $[CO_2]$ values shown are rounded down to integral numbers for clarity. More detailed information can be found in Section 2.

studies from Song et al. (2019) and Terrer et al. (2019). We screened all these data using the following criteria: (1) experiments containing fertilized/high water/high temperature/drought treatments were all excluded because of the interactions; (2) measurements from the same experiment but different years were not independent, so only observations in the last year were selected; (3) different species in the same experiment were considered independent; and (4) experiments were only included when both above- and below-ground biomass per unit area were provided. A factor of 0.5 was used to convert dry-matter content to carbon content. In total, we compiled 41 plant biomass data (under the elevated $[CO_2]$ and control treatments) from 24 $CO_2$-enrichment experiments (Figure S1; Table S1). For each site, the response of plant biomass to increasing $[CO_2]$ ($\beta^{Obs}_{Site}$) was then estimated as:

$$\beta^{Obs}_{Site} = \frac{Biomass_T - Biomass_C}{CO_2^T - CO_2^C}, \quad (1)$$

where $Biomass_T$ and $Biomass_C$ are the values of observed plant biomass C density under elevated $[CO_2]$ treatment ($CO_2^T$) and control ambient concentration ($CO_2^C$) during the experiment, respectively. Both $CO_2^T$ and $CO_2^C$ were likely different among the experimental sites (Table S1). Note that $CO_2^T$ was approximately twofold higher than preindustrial levels (~286.46 ppm in 1850), because the general purpose of the $CO_2$-enrichment experiments was to realistically simulate future $[CO_2]$ and analyze the response of plant biomass to elevated $[CO_2]$ above current levels (Walker et al., 2021).

## 2.3 | Simulated CFE on plant biomass from an ensemble of DGVMs

We used the outputs of biomass C stock (variable 'cVeg') during 1850–2019 from an ensemble of 10 DGVMs in the TRENDYv9 project (CABLE-POP, DLEM, IBIS, ISAM, ISBA-CTRIP, JSBACH, JULES-ES-1.0, LPJ-GUESS, LPX-Bern, and ORCHIDEEv3). All DGVMs were coordinated to perform consistent factorial simulations based on the TRENDY intercomparison protocol using the same climate forcings, increasing atmospheric $[CO_2]$, and products of changes in land use and land cover (Ballantyne et al., 2012; Sitch et al., 2015). All modeled outputs were resampled to a common spatial resolution of 0.5°×0.5° using the nearest neighbor method.

We first extracted the CFE-induced change in biomass over time (written here as Biomass) as the difference in simulated cVeg between the S1 (time-varying $[CO_2]$ only) and S0 (constant $[CO_2]$) simulations

for each model. The simulated response of plant biomass to increasing $[CO_2]$ in NHee ($\beta^{Mod}_{NHee}$) for each model was then calculated as:

$$\beta^{Mod}_{NHee} = \frac{Biomass_{Last} - Biomass_{First}}{CO_2^{Last} - CO_2^{First}}, \quad (2)$$

where $Biomass_{Last}$ and $Biomass_{First}$ represent the area-weighted average of CFE-induced change in biomass C density (S1–S0) in NHee for the last year and the first year of the simulated period, respectively, $CO_2^{Last}$ and $CO_2^{First}$ represent the atmospheric $[CO_2]$ for the last year and the first year of the simulated period, respectively. The first year was 1850 when estimating $\beta^{Mod}_{NHee}$ for 1850–2019 and was 1990 when estimating $\beta^{Mod}_{NHee}$ for 1990–2019. We applied the same approach to further estimate the response of plant biomass C density to increasing $[CO_2]$ for different biomes (Figure S2) and different countries/regions ($\beta^{Mod}_{Reg}$, Figures S3–S8).

## 2.4 | Conversion of simulated site-scale CFE on plant biomass with a gradual increase in $[CO_2]$ to a step increase in $[CO_2]$

Atmospheric $[CO_2]$ increased gradually in the DGVMs, similar to the real world, but increased abruptly in the $CO_2$-enrichment experiments (Figure 1). To align the $[CO_2]$ changes in the models with the data, we used a two-box model (Liu et al., 2019) to transform the gradual increase in $[CO_2]$ for each DGVM to replicate the step increase in $[CO_2]$ at the experimental sites.

First, we obtained the simulated CFE-induced change in net primary productivity (NPP) and biomass C density (S1–S0) for 1850–2019 for each experimental site and each model by averaging the simulated values within a 4.5°×4.5° window around the corresponding site. Our choice of the window size was adopted from Liu et al. (2019). We assumed that the turnover rate of the biomass C pool ($\mu$) was constant, so the change in biomass C density resulted from the change in NPP could be represented by:

$$\frac{d\Delta Biomass(i)}{di} = NPP(i) - \mu \Delta Biomass(i), \quad (3)$$

where $\Delta Biomass(i)$ is the CFE-induced change in biomass C density (S1–S0) in year $i$ relative to the first year, and $NPP(i)$ is the CFE-induced mean annual NPP (S1–S0) in year $i$.

We then calculated the analytical solution to Equation (3) as:

$$\Delta Biomass(i) = \int_0^i \left[\exp(-\mu i')\times NPP(i-i')\right] di'. \quad (4)$$

Second, the original simulated ΔBiomass and NPP for 1850–2019 were used to fit the parameter $\mu$ for each site and each model based on Equation (4). As a result, site-scale ΔBiomass ($\Delta Biomass_{site}$) emulated by the two-box model generally agreed well with the original simulated $\Delta Biomass_{site}$ in most of the DGVMs, indicating that the fitted parameter $\mu$ could be used to represent the turnover rate of biomass in this study (Figure S9).

Third, we assumed that $[CO_2]$ increased abruptly from $CO_2^{First}$ to $CO_2^{Last}$ and then remained stable during the simulation period for each experimental site and each model, that is, simulated NPP would also increase abruptly in response to increasing $[CO_2]$, which was assumed to be constant during the experimental period ($i$ in Equation 4) and calculated as the difference between the CFE-induced mean annual NPP under $CO_2^{Last}$ and $CO_2^{First}$. $\Delta Biomass_{site}$ for each model could thus be reproduced using Equation (4), applying the constant parameter $\mu$ obtained above. At last, the simulated site-scale CFE on plant biomass C density ($\beta^{Mod}_{Site}$) was equal to $\Delta Biomass_{site}$ divided by the difference between $CO_2^{Last}$ and $CO_2^{First}$ (Equation 2).

## 2.5 | Conversion of observed site-scale CFE on plant biomass at future $[CO_2]$ to CFE at historical $[CO_2]$

The difference in atmospheric $[CO_2]$ between the control (e.g., about 380 ppm) and elevated $[CO_2]$ treatments (e.g. about 610 ppm) in the $CO_2$-enrichment experiments was much larger than the difference in the DGVMs (e.g., from 286.46 ppm in 1850 to 409.39 ppm in 2019), preventing the direct comparison between the DGVMs and the $CO_2$-enrichment experiments (Figure 1). To transform the observed CFE on plant biomass at future $[CO_2]$ levels in the experiments to that at historical $[CO_2]$ levels, we needed to extrapolate the change in plant biomass from $CO_2^C$ to $CO_2^T$ to the change in plant biomass from $CO_2^{First}$ to $CO_2^{Last}$.

Assuming that the turnover rates of the biomass C pool were unchanged with an increase in $[CO_2]$ in the DGVMs (Figure S10), changes in biomass caused by a step increase in $[CO_2]$ at historical ($\Delta Biomass^{Hist}_{Site}$) and future ($\Delta Biomass^{Obs}_{Site}$) $[CO_2]$ levels could be calculated using Equation (4) as:

$$\Delta Biomass^{Hist}_{Site}(i) = \int_0^i \left[\exp(-\mu i')\times NPP^{Hist}_{Site}(i-i')\right] di', \quad (5)$$

$$\Delta Biomass^{Obs}_{Site}(i) = \int_0^i \left[\exp(-\mu i')\times NPP^{Obs}_{Site}(i-i')\right] di', \quad (6)$$

thus,

$$\Delta Biomass^{Hist}_{Site}(i) = \frac{\Delta NPP^{Hist}_{Site}}{\Delta NPP^{Obs}_{Site}} \times \Delta Biomass^{Obs}_{Site}(i), \quad (7)$$

where $\Delta NPP^{Hist}_{Site}$ and $\Delta NPP^{Obs}_{Site}$ are changes in CFE-induced NPP at historical and future $[CO_2]$, respectively. C-use efficiency (CUE, the ratio of NPP to gross primary productivity (GPP)) was assumed to be constant across historical and future $[CO_2]$ in the models (Figure S11), so the site-scale CFE on plant biomass C density at historical $[CO_2]$ ($\beta^{Hist}_{Site}$) could be expressed as:

$$\beta^{Hist}_{Site} = \frac{\Delta Biomass^{Hist}_{Site}}{CO_2^{Last} - CO_2^{First}} = \frac{\frac{\Delta NPP^{Hist}_{Site}}{CO_2^{Last} - CO_2^{First}} / CUE}{\frac{\Delta NPP^{Obs}_{Site}}{CO_2^{T} - CO_2^{C}} / CUE} \times \frac{\Delta Biomass^{Obs}_{Site}}{CO_2^{T} - CO_2^{C}} = \frac{\frac{\Delta GPP^{Hist}_{Site}}{CO_2^{Last} - CO_2^{First}}}{\frac{\Delta GPP^{Obs}_{Site}}{CO_2^{T} - CO_2^{C}}} \times \beta^{Obs}_{Site}, \quad (8)$$

where $\Delta GPP_{Site}^{Hist}$ and $\Delta GPP_{Site}^{Obs}$ are changes in CFE-induced GPP at historical and future [$CO_2$], respectively, which could be simulated using an optimality-based model of light-use efficiency (P-model; Wang et al., 2017).

The validity of the P-model for predicting GPP has been successfully evaluated based on extensive measurements of ecosystem flux and field studies (Wang et al., 2017). The rpmodel R package provides us with a simple but effective way to estimate CFE-induced GPP change under historical and future [$CO_2$] on the basis of several environmental variables (Table S2). A summary of how the P-model derives $CO_2$ fertilization effects is provided in Supporting Information. The underlying optimality assumption of the P-model implies that it can represent the effects of climate (e.g., temperature, water vapor pressure deficit, atmospheric pressure) based on the first principles rather than imposed empirical functions. The formulation of the P-model thus allows us to account for the $CO_2$ fertilization effects on the LUE, which were mainly ignored in previous LUE frameworks (De Kauwe et al., 2016). We simulated GPP for each site at four [$CO_2$] ($CO_2^{Last}$, $CO_2^{First}$, $CO_2^{T}$, and $CO_2^{C}$) based on the P-model corresponding to the sampling years in the $CO_2$-enrichment experiments (Table S1). $\Delta GPP_{Site}^{Obs}$ and $\Delta GPP_{Site}^{Hist}$ in Equation (8) were thus equal to the difference between $GPP_T$ and $GPP_C$ and between $GPP_{Last}$ and $GPP_{First}$, respectively. Based on this, the observed site-scale CFE on plant biomass at future [$CO_2$] levels ($\beta_{Site}^{Obs}$) can be extrapolated to the CFE at historical [$CO_2$] levels ($\beta_{Site}^{Hist}$). We note that there is a substantial geographical spread in $\beta_{Site}^{Hist}$, with a small proportion of observations yielding negative values.

To conduct further emergent constraint analysis, it is essential to obtain the cross-site-average $\beta_{Site}^{Hist}$ and its corresponding uncertainty. This can be accomplished through a bootstrap resampling approach. First, we randomly selected one $\beta_{Site}^{Hist}$ from each site and then averaged all selected $\beta_{Site}^{Hist}$ across sites. Second, we repeated the first step 1000 times to generate a sample of 1000 $\beta_{Site}^{Hist}$. Third, we calculated the mean ($\overline{\beta}_{Site}^{Hist}$) and standard deviation $\left[\sigma\left(\beta_{Site}^{Hist}\right)\right]$ of all the 1000 $\beta_{Site}^{Hist}$ samples, assuming a Gaussian distribution for all observations.

## 2.6 | Emergent constraints of CFE on plant biomass

The concept of emergent constraint is founded on the premise that the ensemble of models may be applicable for establishing a heuristic relationship between a variable that can be directly measured/observed and another (i.e., the variable of interest) that cannot, even though large uncertainties remain between models (Cox et al., 2013). To constrain the response of plant biomass C density to increasing [$CO_2$] in NHee, we first used least-squares linear regression to assess the relationship between $\beta_{Site}^{Mod}$ and $\beta_{NHee}^{Mod}$ across the ensemble of DGVMs, defined as:

$$\beta_{NHee}^{Mod} = a\,\beta_{Site}^{Mod} + b, \tag{9}$$

where $a$ is the slope and $b$ is the intercept of the regression line, respectively.

The least-squares error of this regression model was calculated as:

$$s^2 = \frac{\sum_{m=1}^{M}\left(\tilde{\beta}_{NHee}^{Mod} - \beta_{NHee}^{Mod}\right)^2}{(M-2)}, \tag{10}$$

where $M$ is the number of DGVMs, $(M-2)$ is the degrees of freedom of the linear regression, and $\tilde{\beta}_{NHee}^{Mod}$ represents the predicted $\beta_{NHee}^{Mod}$ based on Equation (9).

We then re-estimated $\beta_{NHee}^{Mod}$ and its uncertainty given the observation-based $\beta_{Site}^{Hist}$. The sum of squared errors of prediction for $\tilde{\beta}_{NHee}^{Mod}\left|\beta_{Site}^{Hist}\right.$ was estimated as:

$$\sigma\left(\tilde{\beta}_{NHee}^{Mod}\left|\beta_{Site}^{Hist}\right.\right)^2 = s^2\left\{1+\frac{1}{M}+\frac{\left(\beta_{Site}^{Hist}-\overline{\beta}_{Site}^{Hist}\right)^2}{M\sigma\left(\beta_{Site}^{Hist}\right)^2}\right\}, \tag{11}$$

where $\overline{\beta}_{Site}^{Hist}$ is the average of series $\beta_{Site}^{Hist}$ across experimental sites.

Assuming a normal distribution of $\tilde{\beta}_{NHee}^{Mod}\left|\beta_{Site}^{Hist}\right.$, the probability density function (PDF) of $\tilde{\beta}_{NHee}^{Mod}$ given $\beta_{Site}^{Hist}$ was:

$$P\left(\tilde{\beta}_{NHee}^{Mod}\left|\beta_{Site}^{Hist}\right.\right) = \frac{1}{\sqrt{2\pi\sigma\left(\tilde{\beta}_{NHee}^{Mod}\left|\beta_{Site}^{Obs}\right.\right)}}\exp\left\{-\frac{\left(\tilde{\beta}_{NHee}^{Mod}-\beta_{NHee}^{Mod}\right)^2}{2\sigma\left(\tilde{\beta}_{NHee}^{Mod}\left|\beta_{Site}^{Mod}\right.\right)}\right\}. \tag{12}$$

The PDF for emergent-constrained $\tilde{\beta}_{NHee}^{Mod}$ could thus be estimated as:

$$P\left(\tilde{\beta}_{NHee}^{Mod}\right) = \int_{-\infty}^{+\infty} P\left(\tilde{\beta}_{NHee}^{Mod}\left|\beta_{Site}^{Hist}\right.\right)P\left(\beta_{Site}^{Hist}\right)\mathrm{d}\beta_{Site}^{Hist}, \tag{13}$$

where $P\left(\beta_{Site}^{Hist}\right)$ is the PDF of the variable $\beta_{Site}^{Hist}$.

We also applied the same method of emergent constraint to explore the model performance in different biomes and different regions/countries separately. Correlating simulated $\beta_{Reg}^{Mod}$ and $\beta_{Site}^{Mod}$ for each of the six major countries/regions, however, was difficult, because not all the regions have the corresponding $CO_2$ experimental sites (Figure S1). We found that simulated $\beta_{Reg}^{Mod}$ in the United States increased linearly across the DGVMs, with both regional site-averaged $\beta_{Site}^{Mod}$ for all temperate-forest sites (Figure S6) and forest sites in the United States only (Figure S12). That is to say, $\beta_{Site}^{Mod}$ of boreal or temperate forests could be used to replace regional $\beta_{Site}^{Mod}$ to correlate with regional CFE-induced increase, as an alternative. We thus used observed site-average $\beta_{Site}^{Hist}$ of boreal and temperate forests to constrain the simulated $\beta_{Reg}^{Mod}$ in boreal (Figures S3–S5) and temperate (Figures S6–S8) countries/regions, respectively.

## 2.7 | Analysis of robustness

The robustness of the constrained CFE on plant biomass was confirmed by reducing the number of experimental sites. We first selected $(n-m)$ experimental sites from a total of $n$ sites to constrain the simulated response in the DGVMs, where $m$ is the number of

experimental sites ($m = 1, 2, 3$) removed before the calculation. We then repeated this step until all combinations were selected. The combinatorial number was $C_n^{n-m} = \frac{n!}{(n-m)!\,(n-(n-m))!}$. Finally, we calculated the mean and standard deviation for all the above combinations to represent the average constrained CFE and its uncertainty.

## 2.8 | Calculation of the observed changes in forest biomass since the 1990s

The observed changes in forest biomass over the last three decades in NHee were collected from an inventory-based study (Pan et al., 2011) and a satellite-based product (Xu et al., 2021), respectively. Since forest inventory data have documented changes in forest area for different countries/regions, both the observed change in the density of biomass C ($\Delta Density_{Obs}$, g C $m^{-2}$ $year^{-1}$) and change in the storage of biomass C ($\Delta Storage_{Obs}$, Tg C $year^{-1}$) for whole NHee and each of the six major countries/regions in NHee were analyzed.

First, we extracted the $\Delta Density_{Obs}$ and $\Delta Storage_{Obs}$ during 1990–2007 from inventories as follows, since the area of forest cover has changed over time:

$$\Delta Density_{Obs} = \frac{\frac{Storage_{2007}}{Area_{2007}} - \frac{Storage_{1990}}{Area_{1990}}}{\Delta year}, \quad (14)$$

$$\Delta Storage_{Obs} = \frac{Storage_{2007} - Storage_{1990}}{\Delta year}, \quad (15)$$

where $Area_{1990}$ and $Area_{2007}$ denote the total forest area for 1990 and 2007, respectively, and $Storage_{1990}$ and $Storage_{2007}$ denote the total storage of biomass C for 1990 and 2007, respectively, all of which could be obtained from tables S2 and S3 in Pan et al. (2011). $\Delta year$ is the length of the study period which is set to 18.

Second, we estimated $\Delta Density_{Obs}$ and $\Delta Storage_{Obs}$ using a newly released satellite-based dataset of global C stocks in woody vegetation during 2000–2019 (Xu et al., 2021). This data set was produced at a spatial resolution of 10 km by compiling a large number of ground inventories, airborne laser scanning, and satellite lidar data to train a self-improving machine-learning model using systematic time series observations from microwave and optical satellite imagery. The conversion of above- to below-ground live biomass was based on vegetation specific root: shoot ratios (see table S5 in Xu et al., 2021). Note that detecting biomass gain in intact forests with high biomass can be challenging due to the "slow in–fast out" characteristic, as well as the potential saturation of satellite signals in dense forest (Harris et al., 2016; Smith et al., 2020). To address this, Xu et al. (2021) established an approach to adjust the long-term estimates of C changes in large-biomass forests. We follow the same approach. We first separate the biomass changes in large-biomass forests (defined as areas with AGB > 100 Mg $ha^{-1}$) and low-biomass forests (defined as areas with AGB ≤ 100 Mg $ha^{-1}$). Specifically, the biomass changes in large-biomass forests were estimated by multiplying the biome-specific growth rates (see table S4 in Xu et al., 2021) by the areas of the regions, whereas the biomass changes in low-biomass forests were estimated using linear regression over time. The sum of the biomass changes in large-biomass forests and low-biomass forests was considered as the $\Delta Storage_{Obs}$. Furthermore, the change in the density of forest biomass C was estimated as $\Delta Density_{Obs} = \frac{\Delta StorageObs}{Area}$, where Area is the total forest area in 2001 in NHee based on MODIS land-cover data, without considering the changes in forest area over time.

## 2.9 | Calculation of the CFE-induced changes in forest biomass since the 1990s

We calculated the CFE-induced changes in the density of biomass C ($\Delta Density_{CFE}$, g C $m^{-2}$ $year^{-1}$) and changes in the storage of biomass C ($\Delta Storage_{CFE}$, Tg C $year^{-1}$) in NHee as follows:

$$\Delta Density_{CFE} = \frac{\beta_{Forest}^{Mod} \times \Delta CO_2}{\Delta year}, \quad (16)$$

$$\Delta Storage_{CFE} = \frac{\beta_{Forest,S}^{Mod} \times \Delta CO_2}{\Delta year}, \quad (17)$$

where $\beta_{Forest}^{Mod}$ is the response of forest biomass C density to increasing $[CO_2]$ in NHee for 1990–2019, $\beta_{Forest,S}^{Mod}$ is the response of forest biomass C storage to increasing $[CO_2]$ in NHee for 1990–2019, $\Delta CO_2$ is the difference in the global atmosphere $[CO_2]$ between 2019 and 1990, and $\Delta year$ is the length of the study period which is set to 30. The uncertainty associated with $\Delta Density_{CFE}$ and $\Delta Storage_{CFE}$ was propagated by the uncertainty associated with $\beta_{Forest}^{Mod}$ and $\beta_{Forest,S}^{Mod}$, respectively.

# 3 | RESULTS

## 3.1 | Constrained CFE on plant biomass in extra-tropical Northern Hemisphere

The simulated response of plant biomass to time-evolving smoothly increasing $[CO_2]$ in the entire NHee ($\beta_{NHee}^{Mod}$) was tightly correlated with the simulated site-average response of plant biomass to short-term step increases in $[CO_2]$ ($\beta_{Site}^{Mod}$) across the DGVMs ($r = .73$, $p = .0175$; Figure 2b). This strong linear relationship confirmed the existence of our proposed emergent constraint, and models with a large site-scale $\beta_{Site}^{Mod}$ also produced a large NHee-scale $\beta_{NHee}^{Mod}$, as expected. Combined with the observed site-average response measurement, with a value at historical $[CO_2]$ levels ($\beta_{Site}^{Hist}$) of 0.29 ± 0.02 kg C $m^{-2}$ [100 ppm]$^{-1}$ (mean ± standard deviation), the model-derived heuristic relationship provided a constrained $\beta_{NHee}^{Mod}$ of 0.49 ± 0.12 kg C $m^{-2}$ [100 ppm]$^{-1}$ for period 1850–2019. This more refined emergent constraint-based $\beta_{NHee}^{Mod}$ was slightly lower than the original multi-model average (0.53 ± 0.15 kg C $m^{-2}$ [100 ppm]$^{-1}$). Furthermore, the relationship shown in Figure 2b generated a constrained PDF of $\beta_{NHee}^{Mod}$, which was narrower than the unconstrained PDF for the

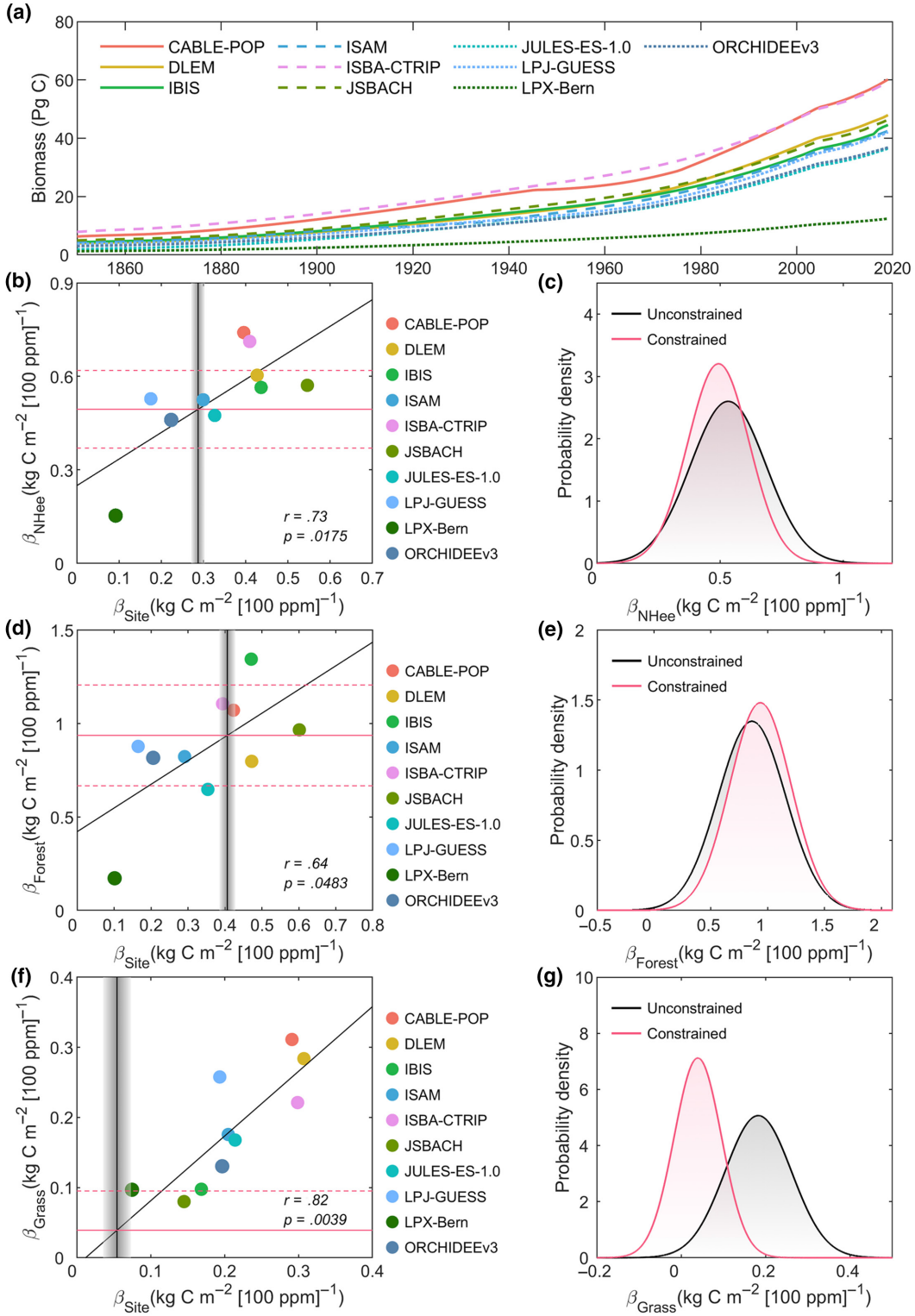


FIGURE 2 Constrained $CO_2$ fertilization effect (CFE) on plant biomass in Northern Hemisphere extra-tropical ecosystems (NHee) during 1850–2019. (a) CFE-induced change in plant biomass during 1850–2019 in the dynamic global vegetation models (DGVMs). Note that changes in plant biomass were all shown with a 30-year moving window for demonstration purposes. (b) Relationship between the simulated response of plant biomass to increasing [$CO_2$] in NHee ($\beta^{Mod}_{NHee}$) and the simulated site-average response of plant biomass to increasing [$CO_2$] ($\beta^{Mod}_{Site}$) across the DGVMs. The vertical gray area represents the observed response of plant biomass to increasing [$CO_2$] from $CO_2$-enrichment experiments ($\beta^{Obs}_{Site}$, mean ± standard deviation). The horizontal pink lines represent the constraint estimate of $\beta^{Mod}_{NHee}$ (solid line) ± standard deviation (dashed lines). (c) Probability density function of $\beta^{Mod}_{NHee}$ before (black line) and after (pink line) constraint. (d–g) Same as (b) and (c) except the field observations of $\beta^{Obs}_{Site}$ are divided into forest and grassland to constrain CFE on plant biomass in (d, e) forest ($\beta^{Mod}_{Forest}$) and (f, g) grassland ($\beta^{Mod}_{Grass}$).

DGVMs, lowering the range of uncertainty of $\beta^{Mod}_{NHee}$ by 20% after constraint (Figure 2c). Additional sensitivity analyses are performed that confirm the robustness of the constrained $\beta^{Mod}_{NHee}$ when using less observational $CO_2$-enrichment sites in the emergent constraint, separately (Figure S13).

We then applied the same method of emergent constraint to explore DGVM performance, and again provided enhanced estimates of fertilization, but disaggregated into two different biomes separately (forest vs. grassland). For forests, the constrained value for $\beta^{Mod}_{Forest}$ was 0.94 ± 0.27 kg C m$^{-2}$ [100 ppm]$^{-1}$ during 1850–2019 ($r$ = .64, $p$ = .0483; Figure 2d), which was about 11% higher than the original multi-model average (0.85 ± 0.28 kg C m$^{-2}$ [100 ppm]$^{-1}$; Figure 2e). For grassland, the constrained $\beta^{Mod}_{Grass}$ value in NHee during 1850–2019 was estimated to be 0.04 ± 0.06 kg C m$^{-2}$ [100 ppm]$^{-1}$ ($r$ = .82, $p$ = .0039; Figure 2f), which, unlike for forest, was much lower (decrease of 78%) than the unconstrained multi-model mean (0.18 ± 0.08 kg C m$^{-2}$ [100 ppm]$^{-1}$; Figure 2g).

## 3.2 | Contribution of CFE to forest biomass change

The growing amount of inventory data and the development of satellite remote sensing enable a rigorous characterization of the growth trajectory of forest biomass over the past three decades (Harris et al., 2021; Liu et al., 2015; Pan et al., 2011; Xu et al., 2021). Such data provided us with an excellent opportunity to examine the contribution of CFE to the observed overall increases in NHee forest biomass (see Section 2). Unlike the $CO_2$-enrichment experiments, which are designed to capture in isolation the impacts of elevated [$CO_2$], the satellite retrievals and inventories capture the trends in plant biomass due to all forcings combined (notably climate change, CFE, N deposition, and land-use change). To match the temporal extent of the biomass observations from inventories (Pan et al., 2011) and satellites (Xu et al., 2021), our emergent constraint analysis of Figure 2 was revisited, but now for a shorter period of years 1990–2019. Using the same data from $CO_2$-enrichment sites, in tandem with the emergent constraint, we obtained a lower response of plant biomass to rising [$CO_2$] in NHee-scale total forests ($\beta^{Mod}_{Forest}$, 0.86 ± 0.28 kg C m$^{-2}$ [100 ppm]$^{-1}$, Figure 3) compared to that for 1850–2019. As before, the robustness of the constrained $\beta^{Mod}_{Forest}$ was confirmed by the analyses using fewer observational $CO_2$-enrichment sites for the emergent constraint (Figure 3; Figure S2). We then multiplied this constrained $\beta^{Mod}_{Forest}$ with a historical $\Delta CO_2$ of 56.19 ppm (from 353.20 in 1990 to 409.39 ppm in 2019), the result indicated that CFE has increased the forest biomass C storage by 248.04 ± 80.87 Tg C year$^{-1}$ ($\Delta Storage_{CFE}$; Figure S14). This CFE-driven change was then compared against the observed total changes ($\Delta Storage_{Obs}$) from our two datasets for biomass. We therefore identified that $CO_2$ fertilization alone explained 54 ± 18% of the observed increase (461.11 Tg C year$^{-1}$) reported from forest inventories over the past three decades (Table S3). Using an independent satellite-derived biomass product, the dominant role of CFE was further confirmed, suggesting a contribution of 64 ± 21% for the same period (Table S3).

The CFE may be different between temperate and boreal forests due to their contrasting environmental limitations (Terrer et al., 2019). Splitting our analysis into these biomes, we found a major difference, where the constrained $\beta^{Mod}_{Temp}$ of 1.04 ± 0.31 kg C m$^{-2}$ [100 ppm]$^{-1}$ for temperate forests was three times the size of the constrained value for boreal forests, $\beta^{Mod}_{Boreal}$ of 0.36 ± 0.26 kg C m$^{-2}$ [100 ppm]$^{-1}$ (Figure 3; Figure S2). Combining these two values with the estimates of satellite-derived biomass increase (country-level inventory data cannot be recalculated to match the regional extent of each biome), the contribution of CFE was found to have made a larger contribution to temperate forests (71 ± 21%) than boreal forests (34 ± 25%).

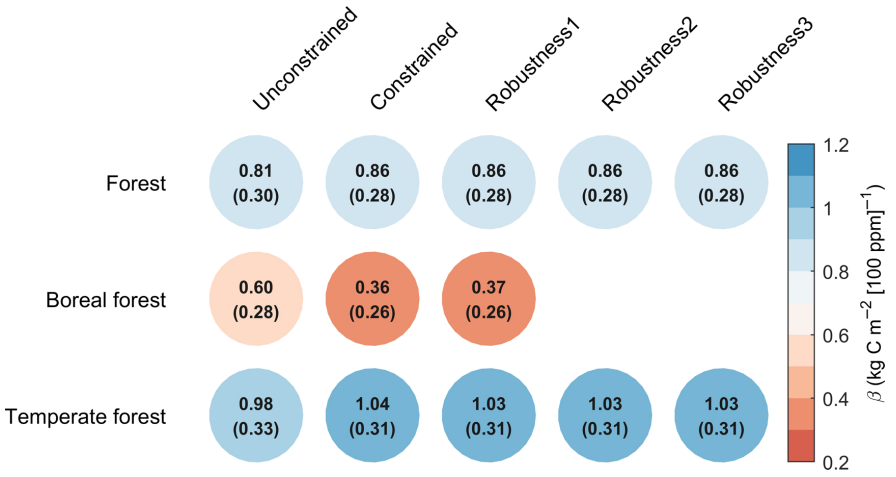


FIGURE 3 Constrained $CO_2$ fertilization effect (CFE) on temperate and boreal forest biomass in Northern Hemisphere extra-tropical ecosystems during 1990–2019. The first number in each circle indicates the multi-model average of originally simulated CFE (Unconstrained), constrained CFE using all observational sites (Constrained) and constrained CFE using one ($Robustness_1$), two ($Robustness_2$), or three ($Robustness_3$) fewer observational sites for total forest, boreal forest, and temperate forest, respectively. The standard deviation of CFE is shown in brackets.

### 3.3 | Regional differences in the contribution of CFE to forest biomass change

Carbon loss and gain in forest biomass may be strongly influenced by direct human disturbance and other environmental changes, which may alter the relative contribution of CFE at the regional scale. To further identify the role of CFE for the six major countries/regions in NHee, that is, Canada, northern Europe, Russia, the United States, temperate Europe, and China, we used the same fractional approach as outlined above (i.e., the calculation of $\Delta Storage_{CFE}/\Delta Storage_{Obs}$; Materials and Methods). Our analyses showed that CFE contributed the most to the inventory-based forest biomass increase in China (56 ± 19%), followed by northern Europe (39 ± 20%), the United States (29 ± 9%), and Russia (28 ± 24%), with a lesser contribution for about 13 ± 5% in temperate Europe (Figure 4; Table S3). Of particular note is that in Canada, a negative contribution of CFE was detected (−117 ± 71%; Figure 4; Table S3). Additional to our analysis based on forest inventory data (black regular triangles in Figure 4), we also examined results from an independent satellite-based biomass dataset (red inverted triangles in Figure 4), which inferred similar or larger proportions of CFE among most countries/regions. These satellite-derived values have some similarities with the estimates from forest inventories, although there are particular differences for temperate Europe.

## 4 | DISCUSSION

By constraining the DGVM simulations against $CO_2$-enrichment experiments, we have shown that the historical response of forest biomass to increasing [$CO_2$] was underestimated by DGVMs (Figure 2d,e). Specifically, this underestimation may be associated with a simulated N-cycle in DGVMs that overly restricts predicted $CO_2$ fertilization on photosynthesis, as models with C–N interactions generally produced a strong and progressive N limitation on net primary production for increasing [$CO_2$]. These models, specifically, may underestimate plant N uptake compared to observations (Zaehle et al., 2014), probably because of the missing simulation of high N uptake through ectomycorrhizal tree–fungal associations (Terrer et al., 2016, 2018). Furthermore, the effect of $CO_2$

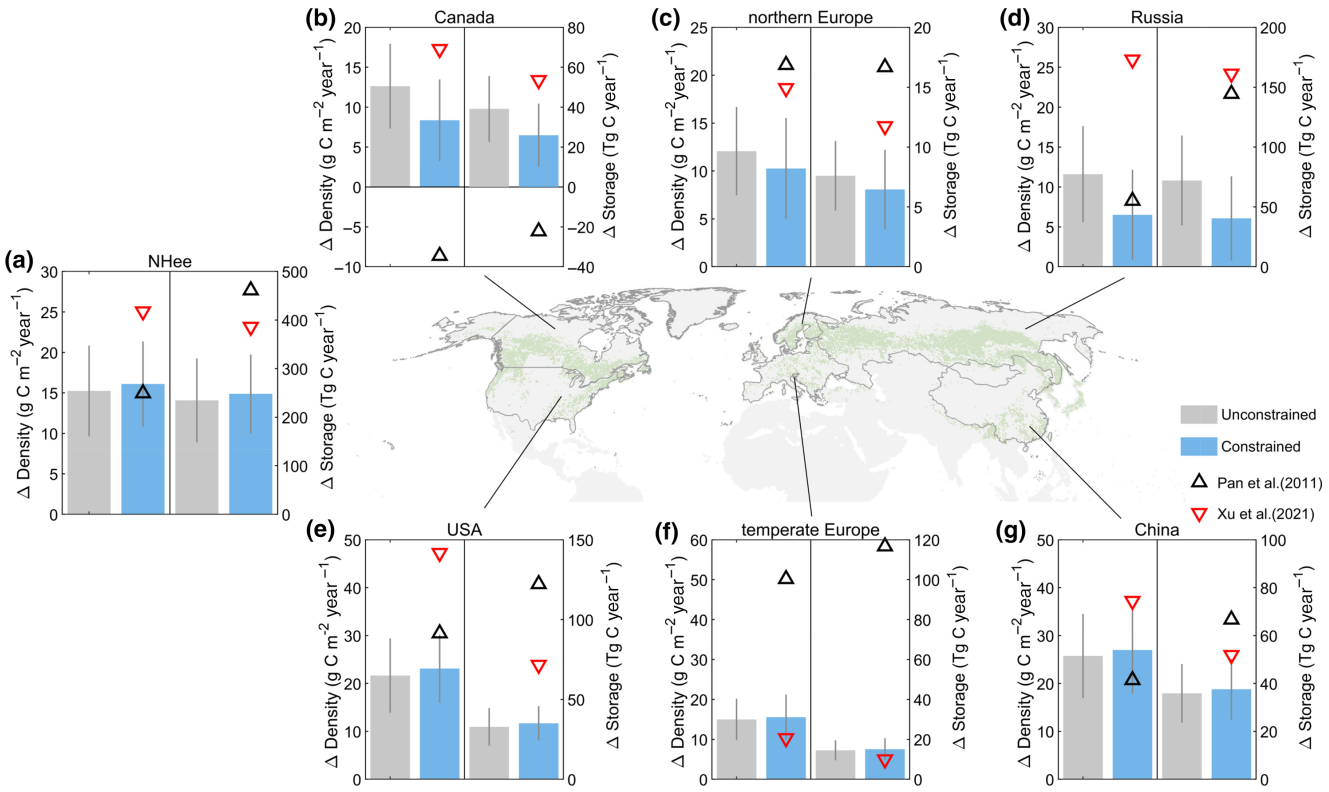


FIGURE 4 Contribution of CFE to changes in forest biomass for Northern Hemisphere extra-tropical ecosystems (NHee) and each of the six major countries/regions since the 1990s. Panels (a) to (g) represent the regions of NHee, Canada, northern Europe, Russia, the United States (USA), temperate Europe, and China, respectively. For each panel, the left side shows the CFE-induced change in the density of biomass carbon ($\Delta Density_{CFE}$), and the right side shows the CFE-induced change in the storage of biomass carbon ($\Delta Storage_{CFE}$). Bars represent the changes in biomass caused by CFE before (gray bars) and after (blue bars) the emergent constraint. The error bars represent the standard deviations of the CFE-induced changes in biomass. Observed changes in biomass carbon density ($\Delta Density_{Obs}$) and storage ($\Delta Storage_{Obs}$) over the last three decades are derived from Pan et al. (2011; black regular triangles) and Xu et al. (2021; red inverted triangles) respectively. The green areas represent forest areas, and the gray areas represent non-forest areas. Map lines delineate study areas and do not necessarily depict accepted national boundaries.

fertilization on plant biomass is dependent on a fine balance between changes in photosynthesis and changes in turnover, where the latter is mainly dependent on the C allocation to different plant components, simulated tissue lifespan as well as whole-plant mortality rates (Koven et al., 2015). Current models focus more on photosynthesis, with a common lack of representation of the mechanisms behind turnover-related processes (Friend et al., 2014; He et al., 2021; Koven et al., 2015; Sullivan et al., 2022). For example, most models estimate an overall higher baseline woody turnover rate, as well as divergent turnover response to rising [$CO_2$], when compared to the observations at Oak Ridge and Duke free-air $CO_2$ enrichment sites. This deficiency in process representation and parameterization further leads to large uncertainties in biomass carbon accumulation (De Kauwe et al., 2014).

In addition, our results show that the historical response of grassland biomass to increasing [$CO_2$] in grassland was generally overestimated by DGVMs (Figure 2f,g). We considered four possible explanations that may account for this major difference. First, grasslands are mainly distributed in temperate regions (Figure S1), where seasonal variations in precipitation could strongly regulate terrestrial plant growth (Hovenden et al., 2014; Obermeier et al., 2017). A previous study suggested that annual CFE on biomass production was largely offset by the opposite response of CFE between the increase in spring and non-spring precipitation (Hovenden et al., 2019), but such mechanism is not considered in current models. Second, most land-surface models have only a limited description of plant functional types, including models for grasses. Recent studies have found that changes in the composition of grassland species due to higher [$CO_2$] may lead to the loss of C, generating a lower (and observed) impact of CFE on grassland biomass (Mueller et al., 2016; Song et al., 2019; Zhu et al., 2020). Third, a global synthesis of $CO_2$ experiments suggested that grasslands tend to accumulate more C in soils, rather than in biomass, when exposed to elevated [$CO_2$] (Terrer et al., 2021). However, this tradeoff, as well as the complex interactions of root–microbe–mineral in grass rhizosphere, are not currently reproduced in models. Finally, our inferred low CFE-induced biomass increases in grassland may be also associated with the low efficiency in N uptake in arbuscular mycorrhizal plants, including grassland species (Terrer et al., 2018), and that once again is not represented in DGVMs. All these possible omissions in models may account for the overestimation of simulated CFE, indicating that the biomass C sink capacity of grassland is far lower than previously expected.

In terms of the contribution of CFE to plant biomass since the 1990s, our findings suggest a larger contribution of CFE in temperate forests compared to boreal forests. This difference could be explained by the stronger limitations on plant growth due to N constraints (Du et al., 2020; Terrer et al., 2019; Vallicrosa et al., 2021) and low temperatures (Keenan & Riley, 2018; Zhu et al., 2016) in boreal ecosystems. However, we also observed a negative contribution of CFE in Canada. One possible reason for this negative contribution is that the storage-based metric ($\Delta Storage_{CFE}/\Delta Storage_{Obs}$) used here is more reliable in regions with substantial increases in forest area (Figure S15), while a density-based metric ($\Delta Density_{CFE}/\Delta Density_{Obs}$) may be better suited for regions undergoing forest loss, that is, Canada. Nevertheless, even when using the density-based metric, the contribution of CFE in Canada was still negative (−97 ± 59%; Figure 4; Table S3). Therefore, we suggested that the negative impacts on forest biomass were primarily due to the significant influence of disturbances in Canadian forests, and in particular pest attacks and wildfires (Kasischke & Turetsky, 2006; Wang et al., 2015). These disturbances were so severe that they exceed any potential positive effects of CFE, as well as any other factors, resulting in a net decrease in forest biomass.

Considering the differences in CFE contribution between satellite- and inventory-based estimates (Table S3), there are several possible explanations. For example, some lack of agreement may be attributable to the differences in the observational periods. The satellite data were integrated over years 2000–2019, and therefore potentially captured more loss of forest biomass C from post-2007 disturbances in boreal and temperate regions (Forzieri et al., 2021; Seidl et al., 2014), which was not captured by the forest inventory data based on the years 1990–2007. In addition, previous studies have suggested that optical and microwave satellite data with short wavelengths may have inadequate sensitivity to detect gradual forest gain, compared with their good ability to observe more abrupt forest loss signals, such as deforestation (Bartels et al., 2016; Li et al., 2017; Tian et al., 2015). This deficiency is more evident in dense forests, where the data may underestimate the increase in observed woody biomass due to CFE-induced increases in light-use efficiency (Smith et al., 2020), and thus result in a greater fraction of CFE contribution.

An additional theoretical possibility of finding low CFE contributions is for regions characterized by large-scale forest areal expansion. A large C accumulation for trees may be expected due to rapid growth through direct afforestation/reforestation (Chen et al., 2019), rather than the fertilization effect, in areas of planting and regrowth. Contrary to expectations, however, the country with the largest gain in forest area (Pan et al., 2011), that is, China, also had the highest percentage contribution of CFE compared to that of other regions (Figure 4; Table S3). We do, though, suggest some caution regarding the robustness of our predicted contributions at the regional scale due to a dearth of sufficient $CO_2$ experiments, including both above- and below-ground information, to adequately constrain regional CFE. Further validation is also necessary, potentially through enhanced spatial sampling with longer-duration $CO_2$-enrichment experiments (Jones et al., 2014).

Furthermore, recent studies have indicated an increasing constraint of climate on vegetation growth, which may ultimately counteract the potential growth benefits of CFE (Green et al., 2019; Jiao et al., 2021; Peñuelas et al., 2017; Yuan et al., 2019). Our analysis revealed a small decrease in constrained CFE for forests from 1850–2019 ($0.94 \pm 0.27\,kg\,C\,m^{-2}\,[100\,ppm]^{-1}$) to 1990–2019 ($0.86 \pm 0.28\,kg\,C\,m^{-2}\,[100\,ppm]^{-1}$), caution should be exercised in drawing conclusions about a decline in CFE solely based on these findings. We note that same site-scale $CO_2$-enrichment observations at future [$CO_2$] levels were used to estimate $\beta_{Site}^{Hist}$ at different historical [$CO_2$] levels (1850–2019 and 1990–2019, respectively; see Section 2).

Additionally, the application of the P-model, as needed to convert site-scale response of GPP to rising [$CO_2$] to expected changes between historical [$CO_2$] levels and future [$CO_2$] levels, contains implicitly a saturation effect over time (Figure 1; Liu et al., 2019), which may eventually result in a predicted slowdown of CFE between the two time periods. Whether the positive effects of CFE on biomass carbon enhancement may be expected to continue to outweigh the negative effects of climate-induced biomass losses in the immediate future remains an important issue to be addressed.

## 5 | CONCLUSION

In summary, our study presents a simple, highly intuitive, and effective approach to determine the magnitude of the large-scale influence of $CO_2$-induced fertilization on plant biomass. Of particular interest is that we have formally isolated the contribution of CFE from other non-CFE drivers. We have achieved this by exploiting multiple observational constraints, dynamical global vegetation models, and an emergent constraint technique to fuse together such observational data and models. Our study indicated that $CO_2$ fertilization is the dominant driver of the observed forest biomass increase over the last decades across the NHee. Specifically, inventory- and satellite-based evidence suggested the fertilization contribution was 54 ± 18% and 64 ± 21%, respectively. Eventually, the positive effect of $CO_2$ fertilization may slow down and saturate in the process of achieving carbon neutrality (Franks et al., 2013; Peñuelas et al., 2017; Piao et al., 2022; Winkler et al., 2021), which will further lower the terrestrial ecosystem C sink capacity. Consequently, the presentation of CFE as a solution for long-term climate mitigation merits caution, potentially requiring additional $CO_2$-offset options (e.g., renewable power utilization, deliberate afforestation/reforestation), to achieve carbon neutrality.

### AUTHOR CONTRIBUTIONS

Shilong Piao and Yongwen Liu designed the research; Yue He and Lingjie Lei performed the analysis and wrote the draft of the manuscript; and all authors contributed to the interpretation of the results and to the text.

### ACKNOWLEDGMENTS

We thank the TRENDY modelers for their simulations. S.P. acknowledges the support from the National Natural Science Foundation of China (41988101). Y.W.L. acknowledges the support from the National Natural Science Foundation of China (42122005) and the Youth Innovation Promotion Association CAS (2019074).

### CONFLICT OF INTEREST STATEMENT

The authors declare no competing interests.

### DATA AVAILABILITY STATEMENT

The main data that support the findings of this study are openly available in Zenodo at https://doi.org/10.5281/zenodo.7948124. The satellite-derived global live vegetation biomass carbon product is available from https://doi.org/10.5281/zenodo.4161694. The MODIS land cover dataset is available from https://lpdaac.usgs.gov/products/mcd12c1v006. TRENDYv9 data is freely available on request from TRENDY coordinator S. Sitch (s.a.sitch@exeter.ac.uk; https://blogs.exeter.ac.uk/trendy/). The P-model is available as an R package (rpmodel, https://cran.r-project.org/package=rpmodel). All other relevant data are available upon request.

### ORCID

*Yue He* https://orcid.org/0000-0002-7754-7026
*Yongwen Liu* https://orcid.org/0000-0002-9664-303X
*Chris Huntingford* https://orcid.org/0000-0002-5941-7770
*Josep Peñuelas* https://orcid.org/0000-0002-7215-0150
*Shilong Piao* https://orcid.org/0000-0001-8057-2292

### REFERENCES

Ballantyne, A. P., Alden, C. B., Miller, J. B., Tans, P. P., & White, J. W. C. (2012). Increase in observed net carbon dioxide uptake by land and oceans during the past 50 years. *Nature*, *488*(7409), 70–72.

Bartels, S. F., Chen, H. Y. H., Wulder, M. A., & White, J. C. (2016). Trends in post-disturbance recovery rates of Canada's forests following wildfire and harvest. *Forest Ecology and Management*, *361*, 194–207.

Chen, C., Park, T., Wang, X., Piao, S., Xu, B., Chaturvedi, R. K., Fuchs, R., Brovkin, V., Ciais, P., & Fensholt, R. (2019). China and India lead in greening of the world through land-use management. *Nature Sustainability*, *2*(2), 122–129.

Cox, P. M., Pearson, D., Booth, B. B., Friedlingstein, P., Huntingford, C., Jones, C. D., & Luke, C. M. (2013). Sensitivity of tropical carbon to climate change constrained by carbon dioxide variability. *Nature*, *494*(7437), 341–344.

De Kauwe, M. G., Keenan, T. F., Medlyn, B. E., Prentice, I. C., & Terrer, C. (2016). Satellite based estimates underestimate the effect of $CO_2$ fertilization on net primary productivity. *Nature Climate Change*, *6*(10), 892–893.

De Kauwe, M. G., Medlyn, B. E., Walker, A. P., Dietze, M. C., Luo, Y., Jain, A. K., El-masri, B., Hickler, T., David, W., Parton, J., Thornton, P. E., Wang, S., Prentice, I. C., Asao, S., Smith, B., Mccarthy, R., Iversen, C. M., Hanson, P. J., Warren, J. M., … Norby, R. J. (2014). Where does the carbon go? A model—Data intercomparison of vegetation carbon allocation and turnover processes at two temperate forest free-air $CO_2$ enrichment sites. *New Phytologist*, *203*, 883–899.

Du, E., Terrer, C., Pellegrini, A. F. A., Ahlström, A., van Lissa, C. J., Zhao, X., Xia, N., Wu, X., & Jackson, R. B. (2020). Global patterns of terrestrial nitrogen and phosphorus limitation. *Nature Geoscience*, *13*(3), 221–226.

Eyring, V., Cox, P. M., Flato, G. M., Gleckler, P. J., Abramowitz, G., Caldwell, P., Collins, W. D., Gier, B. K., Hall, A. D., Hoffman, F. M., Hurtt, G. C., Jahn, A., Jones, C. D., Klein, S. A., Krasting, J. P., Kwiatkowski, L., Lorenz, R., Maloney, E., Meehl, G. A., … Williamson, M. S. (2019). Taking climate model evaluation to the next level. *Nature Climate Change*, *9*(2), 102–110.

Fernández-Martínez, M., Sardans, J., Chevallier, F., Ciais, P., Obersteiner, M., Vicca, S., Canadell, J. G., Bastos, A., Friedlingstein, P., Sitch, S., Piao, S. L., Janssens, I. A., & Peñuelas, J. (2019). Global trends in carbon sinks and their relationships with $CO_2$ and temperature. *Nature Climate Change*, *9*(1), 73–79.

Forzieri, G., Girardello, M., Ceccherini, G., Spinoni, J., Feyen, L., Hartmann, H., Beck, P. S. A., Camps-Valls, G., Chirici, G., Mauri, A., & Cescatti, A. (2021). Emergent vulnerability to climate-driven disturbances in European forests. *Nature Communications*, *12*, 1081.

Franks, P. J., Adams, M. A., Amthor, J. S., Barbour, M. M., Berry, J. A., Ellsworth, D. S., Farquhar, G. D., Ghannoum, O., Lloyd, J., McDowell, N., Norby, R. J., Tissue, D. T., & von Caemmerer, S. (2013). Sensitivity of plants to changing atmospheric $CO_2$ concentration: From the geological past to the next century. *New Phytologist*, *197*(4), 1077–1094.

Friedlingstein, P., O'Sullivan, M., Jones, M. W., Andrew, R. M., Hauck, J., Olsen, A., Peters, G. P., Peters, W., Pongratz, J., Sitch, S., Le Quéré, C., Canadell, J. G., Ciais, P., Jackson, R. B., Alin, S., Aragão, L. E. O. C., Arneth, A., Arora, V., Bates, N. R., … Zaehle, S. (2020). Global carbon budget 2020. *Earth System Science Data*, *12*(4), 3269–3340.

Friend, A. D., Lucht, W., Rademacher, T. T., Keribin, R., Betts, R., Cadule, P., Ciais, P., Clark, D. B., Dankers, R., Falloon, P. D., Ito, A., Kahana, R., Kleidon, A., Lomas, M. R., Nishina, K., Ostberg, S., Pavlick, R., Peylin, P., Schaphoff, S., … Woodward, F. I. (2014). Carbon residence time dominates uncertainty in terrestrial vegetation responses to future climate and atmospheric $CO_2$. *Proceedings of the National Academy of Sciences of the United States of America*, *111*(9), 3280–3285.

Green, J. K., Seneviratne, S. I., Berg, A. M., Findell, K. L., Hagemann, S., Lawrence, D. M., & Gentine, P. (2019). Large influence of soil moisture on long-term terrestrial carbon uptake. *Nature*, *565*(7740), 476–479.

Harris, N. L., Gibbs, D. A., Baccini, A., Birdsey, R. A., de Bruin, S., Farina, M., Fatoyinbo, L., Hansen, M. C., Herold, M., Houghton, R. A., Potapov, P. V., Suarez, D. R., Roman-Cuesta, R. M., Saatchi, S. S., Slay, C. M., Turubanova, S. A., & Tyukavina, A. (2021). Global maps of twenty-first century forest carbon fluxes. *Nature Climate Change*, *11*(3), 234–240.

Harris, N. L., Hagen, S. C., Saatchi, S. S., Pearson, T. R. H., Woodall, C. W., Domke, G. M., Braswell, B. H., Walters, B. F., Brown, S., Salas, W., Fore, A., & Yu, Y. (2016). Attribution of net carbon change by disturbance type across forest lands of the conterminous United States. *Carbon Balance and Management*, *11*(1), 24.

Haverd, V., Smith, B., Canadell, J. G., Cuntz, M., Mikaloff-Fletcher, S., Farquhar, G., Woodgate, W., Briggs, P. R., & Trudinger, C. M. (2020). Higher than expected $CO_2$ fertilization inferred from leaf to global observations. *Global Change Biology*, *26*(4), 2390–2402.

He, Y., Peng, S., Liu, Y., Li, X., Wang, K., Ciais, P., Arain, M. A., Fang, Y., Fisher, J. B., Goll, D., Hayes, D., Huntzinger, D. N., Ito, A., Jain, A. K., Janssens, I. A., Mao, J., Matteo, C., Michalak, A. M., Peng, C., … Zhu, Q. (2020). Global vegetation biomass production efficiency constrained by models and observations. *Global Change Biology*, *26*(3), 1474–1484.

He, Y., Wang, X., Wang, K., Tang, S., Xu, H., Chen, A., Ciais, P., Li, X., Peñuelas, J., & Piao, S. (2021). Data-driven estimates of global litter production imply slower vegetation carbon turnover. *Global Change Biology*, *27*(8), 1678–1688.

Hovenden, M. J., Leuzinger, S., Newton, P. C. D., Fletcher, A., Fatichi, S., Lüscher, A., Reich, P. B., Andresen, L. C., Beier, C., Blumenthal, D. M., Chiariello, N. R., Dukes, J. S., Kellner, J., Hofmockel, K., Niklaus, P. A., Song, J., Wan, S., Classen, A. T., & Langley, J. A. (2019). Globally consistent influences of seasonal precipitation limit grassland biomass response to elevated $CO_2$. *Nature Plants*, *5*(2), 167–173.

Hovenden, M. J., Newton, P. C. D., & Wills, K. E. (2014). Seasonal not annual rainfall determines grassland biomass response to carbon dioxide. *Nature*, *511*(7511), 583–586.

Huntzinger, D. N., Michalak, A. M., Schwalm, C., Ciais, P., King, A. W., Fang, Y., Schaefer, K., Wei, Y., Cook, R. B., Fisher, J. B., Hayes, D., Huang, M., Ito, A., Jain, A. K., Lei, H., Lu, C., Maignan, F., Mao, J., Parazoo, N., … Zhao, F. (2017). Uncertainty in the response of terrestrial carbon sink to environmental drivers undermines carbon-climate feedback predictions. *Scientific Reports*, *7*(1), 4765.

Jiao, W., Wang, L., Smith, W. K., Chang, Q., Wang, H., & D'Odorico, P. (2021). Observed increasing water constraint on vegetation growth over the last three decades. *Nature Communications*, *12*, 3777.

Jones, A. G., Scullion, J., Ostle, N., Levy, P. E., & Gwynn-Jones, D. (2014). Completing the FACE of elevated $CO_2$ research. *Environment International*, *73*, 252–258.

Kasischke, E. S., & Turetsky, M. R. (2006). Recent changes in the fire regime across the north American boreal region—Spatial and temporal patterns of burning across Canada and Alaska. *Geophysical Research Letters*, *33*(9), L09703. https://doi.org/10.1029/2006GL025677

Keenan, T. F., & Riley, W. J. (2018). Greening of the land surface in the world's cold regions consistent with recent warming. *Nature Climate Change*, *8*(September), 825–829.

Koven, C. D., Chambers, J. Q., Georgiou, K., Knox, R., Negron-Juarez, R., Riley, W. J., Arora, V. K., Brovkin, V., Friedlingstein, P., & Jones, C. D. (2015). Controls on terrestrial carbon feedbacks by productivity versus turnover in the CMIP5 Earth System Models. *Biogeosciences*, *12*(17), 5211–5228.

Li, Y., Sulla-Menashe, D., Motesharrei, S., Song, X. P., Kalnay, E., Ying, Q., Li, S., & Ma, Z. (2017). Inconsistent estimates of forest cover change in China between 2000 and 2013 from multiple datasets: Differences in parameters, spatial resolution, and definitions. *Scientific Reports*, *7*(1), 1–12.

Lian, X., Piao, S., Huntingford, C., Li, Y., Zeng, Z., Wang, X., Ciais, P., Mcvicar, T. R., Peng, S., Ottlé, C., Yang, H., Yang, Y., Zhang, Y., & Wang, T. (2018). Partitioning global land evapotranspiration using CMIP5 models constrained by observations. *Nature Climate Change*, *8*, 640–646.

Liu, Y., Piao, S., Gasser, T., Ciais, P., Yang, H., Wang, H., Keenan, T. F., Huang, M., Wan, S., Song, J., Wang, K., Janssens, I. A., Peñuelas, J., Huntingford, C., Wang, X., Altaf Arain, M., Fang, Y., Fisher, J. B., Huang, M., … Wang, T. (2019). Field-experiment constraints on the enhancement of the terrestrial carbon sink by $CO_2$ fertilization. *Nature Geoscience*, *12*(10), 809–814.

Liu, Y. Y., Van Dijk, A. I. J. M., De Jeu, R. A. M., Canadell, J. G., McCabe, M. F., Evans, J. P., & Wang, G. (2015). Recent reversal in loss of global terrestrial biomass. *Nature Climate Change*, *5*(5), 470–474.

McCarthy, H. R., Oren, R., Johnsen, K. H., Gallet-Budynek, A., Pritchard, S. G., Cook, C. W., Ladeau, S. L., Jackson, R. B., & Finzi, A. C. (2010). Re-assessment of plant carbon dynamics at the Duke free-air $CO_2$ enrichment site: Interactions of atmospheric [$CO_2$] with nitrogen and water availability over stand development. *New Phytologist*, *185*(2), 514–528.

Mueller, K. E., Blumenthal, D. M., Pendall, E., Carrillo, Y., Dijkstra, F. A., Williams, D. G., Follett, R. F., & Morgan, J. A. (2016). Impacts of warming and elevated $CO_2$ on a semi-arid grassland are non-additive, shift with precipitation, and reverse over time. *Ecology Letters*, *19*(8), 956–966.

Norby, R. J., Warren, J. M., Iversen, C. M., Medlyn, B. E., & McMurtrie, R. E. (2010). $CO_2$ enhancement of forest productivity constrained by limited nitrogen availability. *Proceedings of the National Academy of Sciences of the United States of America*, *107*(45), 19368–19373.

Obermeier, W. A., Lehnert, L. W., Kammann, C. I., Müller, C., Grünhage, L., Luterbacher, J., Erbs, M., Moser, G., Seibert, R., Yuan, N., & Bendix, J. (2017). Reduced $CO_2$ fertilization effect in temperate C3 grasslands under more extreme weather conditions. *Nature Climate Change*, *7*(2), 137–141.

Pan, Y., Birdsey, R. A., Fang, J., Houghton, R., Kauppi, P. E., Kurz, W. A., Phillips, O. L., Shvidenko, A., Lewis, S. L., Canadell, J. G., Ciais, P., Jackson, R. B., Pacala, S. W., McGuire, A. D., Piao, S., Rautiainen, A., Sitch, S., & Hayes, D. (2011). A large and persistent carbon sink in the world's forests. *Science*, *333*(6045), 988–993.

Peñuelas, J., Ciais, P., Canadell, J. G., Janssens, I. A., Fernández-Martínez, M., Carnicer, J., Obersteiner, M., Piao, S., Vautard, R., & Sardans, J. (2017). Shifting from a fertilization-dominated to a warming-dominated period. *Nature Ecology & Evolution*, *1*(10), 1438–1445.

Peylin, P., Law, R. M., Gurney, K. R., Chevallier, F., Jacobson, A. R., Maki, T., Niwa, Y., Patra, P. K., Peters, W., Rayner, P. J., Rödenbeck, C., Van Der Laan-Luijkx, I. T., & Zhang, X. (2013). Global atmospheric carbon budget: Results from an ensemble of atmospheric $CO_2$ inversions. *Biogeosciences*, *10*(10), 6699–6720.

Piao, S., Sitch, S., Ciais, P., Friedlingstein, P., Peylin, P., Wang, X., Ahlström, A., Anav, A., Canadell, J. G., Cong, N., Huntingford, C., Jung, M., Levis, S., Levy, P. E., Li, J., Lin, X., Lomas, M. R., Lu, M., Luo, Y., … Zeng, N. (2013). Evaluation of terrestrial carbon cycle models for their response to climate variability and to $CO_2$ trends. *Global Change Biology*, *19*(7), 2117–2132.

Piao, S., Wang, X., Park, T., Chen, C., Lian, X., He, Y., Bjerke, J. W., Chen, A., Ciais, P., Tømmervik, H., Nemani, R. R., & Myneni, R. B. (2020). Characteristics, drivers and feedbacks of global greening. *Nature Reviews Earth & Environment*, *1*, 14–27.

Piao, S., Yue, C., Ding, J., & Guo, Z. (2022). Perspectives on the role of terrestrial ecosystems in the 'carbon neutrality' strategy. *Science China Earth Sciences*, *65*(6), 1178–1186.

Reich, P. B., Hobbie, S. E., Lee, T. D., Rich, R., Pastore, M. A., & Worm, K. (2020). Synergistic effects of four climate change drivers on terrestrial carbon cycling. *Nature Geoscience*, *13*(12), 787–793.

Schimel, D., Stephens, B. B., & Fisher, J. B. (2015). Effect of increasing $CO_2$ on the terrestrial carbon cycle. *Proceedings of the National Academy of Sciences of the United States of America*, *112*(2), 436–441.

Seidl, R., Schelhaas, M. J., Rammer, W., & Verkerk, P. J. (2014). Increasing forest disturbances in Europe and their impact on carbon storage. *Nature Climate Change*, *4*(9), 806–810.

Shevliakova, E., Stouffer, R. J., Malyshev, S., Krasting, J. P., Hurtt, G. C., & Pacala, S. W. (2013). Historical warming reduced due to enhanced land carbon uptake. *Proceedings of the National Academy of Sciences of the United States of America*, *110*(42), 16730–16735.

Sitch, S., Friedlingstein, P., Gruber, N., Jones, S. D., Murray-Tortarolo, G., Ahlström, A., Doney, S. C., Graven, H., Heinze, C., & Huntingford, C. (2015). Recent trends and drivers of regional sources and sinks of carbon dioxide. *Biogeosciences*, *12*(3), 653–679.

Smith, W. K., Fox, A. M., MacBean, N., Moore, D. J. P., & Parazoo, N. C. (2020). Constraining estimates of terrestrial carbon uptake: New opportunities using long-term satellite observations and data assimilation. *New Phytologist*, *225*(1), 105–112.

Song, J., Wan, S., Piao, S., Knapp, A. K., Classen, A. T., Vicca, S., Ciais, P., Hovenden, M. J., Leuzinger, S., Beier, C., Kardol, P., Xia, J., Liu, Q., Ru, J., Zhou, Z., Luo, Y., Guo, D., Adam Langley, J., Zscheischler, J., … Zheng, M. (2019). A meta-analysis of 1,119 manipulative experiments on terrestrial carbon-cycling responses to global change. *Nature Ecology & Evolution*, *3*(9), 1309–1320.

Sullivan, M. O., Friedlingstein, P., Sitch, S., Anthoni, P., Arneth, A., Arora, V. K., Bastrikov, V., Delire, C., Goll, D. S., Jain, A., Kato, E., Kennedy, D., Knauer, J., & Lienert, S. (2022). Process-oriented analysis of dominant sources of uncertainty in the land carbon sink. *Nature Communications*, *13*, 4748.

Tagesson, T., Schurgers, G., Horion, S., Ciais, P., Tian, F., Brandt, M., Ahlström, A., Wigneron, J., Ardö, J., Olin, S., Fan, L., Wu, Z., & Fensholt, R. (2020). Recent divergence in the contributions of tropical and boreal forests to the terrestrial carbon sink. *Nature Ecology & Evolution*, *4*(2), 202–209.

Terrer, C., Jackson, R. B., Prentice, I. C., Keenan, T. F., Kaiser, C., Vicca, S., Fisher, J. B., Reich, P. B., Stocker, B. D., Hungate, B. A., Peñuelas, J., McCallum, I., Soudzilovskaia, N. A., Cernusak, L. A., Talhelm, A. F., Van Sundert, K., Piao, S., Newton, P. C. D., Hovenden, M. J., … Franklin, O. (2019). Nitrogen and phosphorus constrain the $CO_2$ fertilization of global plant biomass. *Nature Climate Change*, *9*(9), 684–689.

Terrer, C., Phillips, R. P., Hungate, B. A., Rosende, J., Pett-Ridge, J., Craig, M. E., van Groenigen, K. J., Keenan, T. F., Sulman, B. N., Stocker, B. D., Reich, P. B., Pellegrini, A. F. A., Pendall, E., Zhang, H., Evans, R. D., Carrillo, Y., Fisher, J. B., Van Sundert, K., Vicca, S., & Jackson, R. B. (2021). A trade-off between plant and soil carbon storage under elevated $CO_2$. *Nature*, *591*(7851), 599–603.

Terrer, C., Vicca, S., Hungate, B. A., Phillips, R. P., & Prentice, I. C. (2016). Mycorrhizal association as a primary control of the $CO_2$ fertilization effect. *Science*, *353*(6294), 72–74.

Terrer, C., Vicca, S., Stocker, B. D., Hungate, B. A., Phillips, R. P., Reich, P. B., Finzi, A. C., & Prentice, I. C. (2018). Ecosystem responses to elevated $CO_2$ governed by plant–soil interactions and the cost of nitrogen acquisition. *New Phytologist*, *217*(2), 507–522.

Tian, F., Fensholt, R., Verbesselt, J., Grogan, K., Horion, S., & Wang, Y. (2015). Evaluating temporal consistency of long-term global NDVI datasets for trend analysis. *Remote Sensing of Environment*, *163*, 326–340.

Vallicrosa, H., Sardans, J., Maspons, J., Zuccarini, P., Fernández-Martínez, M., Bauters, M., Goll, D. S., Ciais, P., Obersteiner, M., Janssens, I. A., & Peñuelas, J. (2021). Global maps and factors driving forest foliar elemental composition: The importance of evolutionary history. *New Phytologist*, *233*(1), 169–181.

Walker, A. P., De Kauwe, M. G., Bastos, A., Belmecheri, S., Georgiou, K., Keeling, R. F., McMahon, S. M., Medlyn, B. E., Moore, D. J. P., Norby, R. J., Zaehle, S., Anderson-Teixeira, K. J., Battipaglia, G., Brienen, R. J. W., Cabugao, K. G., Cailleret, M., Campbell, E., Canadell, J. G., Ciais, P., … Zuidema, P. A. (2021). Integrating the evidence for a terrestrial carbon sink caused by increasing atmospheric $CO_2$. *New Phytologist*, *229*(5), 2413–2445.

Wang, H., Prentice, I. C., Keenan, T. F., Davis, T. W., Wright, I. J., Cornwell, W. K., Evans, B. J., & Peng, C. (2017). Towards a universal model for carbon dioxide uptake by plants. *Nature Plants*, *3*(9), 734–741.

Wang, X., Thompson, D. K., Marshall, G. A., Tymstra, C., Carr, R., & Flannigan, M. D. (2015). Increasing frequency of extreme fire weather in Canada with climate change. *Climatic Change*, *130*(4), 573–586.

Wenzel, S., Cox, P. M., Eyring, V., & Friedlingstein, P. (2016). Projected land photosynthesis constrained by changes in the seasonal cycle of atmospheric $CO_2$. *Nature*, *538*(7626), 499–501.

Winkler, A. J., Myneni, R. B., Hannart, A., Sitch, S., Haverd, V., Lombardozzi, D., Arora, V. K., Pongratz, J., Nabel, J. E. M. S., Goll, D. S., Kato, E., Tian, H., Arneth, A., Friedlingstein, P., Jain, A. K., Zaehle, S., & Brovkin, V. (2021). Slowdown of the greening trend in natural vegetation with further rise in atmospheric $CO_2$. *Biogeosciences*, *18*(17), 4985–5010.

Xu, L., Saatchi, S. S., Yang, Y., Yu, Y., Pongratz, J., Bloom, A. A., Bowman, K., Worden, J., Liu, J., Yin, Y., Domke, G., McRoberts, R. E., Woodall, C., Nabuurs, G., De-Miguel, S., Keller, M., Harris, N., Maxwell, S., & Schimel, D. (2021). Changes in global terrestrial live biomass over the 21st century. *Science Advances*, *7*(27), eabe9829.

Yuan, W., Zheng, Y., Piao, S., Ciais, P., Lombardozzi, D., Wang, Y., Ryu, Y., Chen, G., Dong, W., Hu, Z., Jain, A. K., Jiang, C., Kato, E., Li, S., Lienert, S., Liu, S., Nabel, J. E. M. S., Qin, Z., Quine, T., … Yang, S. (2019). Increased atmospheric vapor pressure deficit reduces global vegetation growth. *Science Advances*, *5*(8), aax1396.

Zaehle, S., Jones, C. D., Houlton, B., Lamarque, J. F., & Robertson, E. (2015). Nitrogen availability reduces CMIP5 projections of twenty-first-century land carbon uptake. *Journal of Climate*, *28*(6), 2494–2511.

Zaehle, S., Medlyn, B. E., De Kauwe, M. G., Walker, A. P., Dietze, M. C., Hickler, T., Luo, Y., Wang, Y., El-Masri, B., Thornton, P., Jain, A., Wang, S., Warlind, D., Weng, E., Parton, W., Iversen, C. M., Gallet-Budynek, A., McCarthy, H., Finzi, A., … Norby, R. J. (2014). Evaluation of 11 terrestrial carbon–nitrogen cycle models against observations from two temperate free-air $CO_2$ enrichment studies. *New Phytologist*, *202*(3), 803–822.

Zhu, J., Zhang, Y., Yang, X., Chen, N., & Jiang, L. (2020). Synergistic effects of nitrogen and $CO_2$ enrichment on alpine grassland biomass and community structure. *New Phytologist*, *228*(4), 1283–1294.

Zhu, Z., Piao, S., Myneni, R. B., Huang, M., Zeng, Z., Canadell, J. G., Ciais, P., Sitch, S., Friedlingstein, P., Arneth, A., Cao, C., Cheng, L., Kato, E., Koven, C., Li, Y., Lian, X., Liu, Y., Liu, R., Mao, J., … Zeng, N. (2016). Greening of the Earth and its drivers. *Nature Climate Change*, *6*(8), 791–795.

## DATA SOURCES

Arnone, J. A., III, & Körner, C. (1995). Soil and biomass carbon pools in model communities of tropical plants under elevated $CO_2$. *Oecologia*, *104*, 61–71.

Barnard, R., Leadley, P. W., Lensi, R., & Barthes, L. (2005). Plant, soil microbial and soil inorganic nitrogen responses to elevated $CO_2$: A study in microcosms of Holcus lanatus. *Acta Oecologica*, *27*, 171–178.

Berntson, G. M., Wayne, P. M., & Bazzaz, F. A. (1997). Below-ground architectural and mycorrhizal responses to elevated $CO_2$ in Betula alleghaniensis populations. *Functional Ecology*, *11*, 684–695.

Casella, E., Soussana, J. F., & Loiseau, P. (1996). Long-term effects of $CO_2$ enrichment and temperature increase on the carbon balance of a temperate grass sward. *Journal of Experimental Botany*, *48*, 1309–1321.

Chen, X., Liu, J., Deng, Q., Yan, J., & Zhang, D. (2012). Effects of elevated $CO_2$ and nitrogen addition on soil organic carbon fractions in a subtropical forest. *Plant and Soil*, *357*, 25–34.

Dieleman, W. I. J., Vicca, S., Dijkstra, F. A., Hagedorn, F., Hovenden, M. J., Larsen, K. S., Morgan, J. A., Volder, A., Beier, C., Dukes, J. S., King, J., Leuzinger, S., Linder, S., Luo, Y., Oren, R., de Angelis, P., Tingey, D., Hoosbeek, M. R., & Janssens, I. A. (2012). Simple additive effects are rare: A quantitative review of plant biomass and soil process responses to combined manipulations of $CO_2$ and temperature. *Global Change Biology*, *18*, 2681–2693.

Gielen, B., Calfapietra, C., Lukac, M., Wittig, V. E., de Angelis, P., Janssens, I. A., Moscatelli, M. C., Grego, S., Cotrufo, M. F., Godbold, D. L., Hoosbeek, M. R., Long, S. P., Miglietta, F., Polle, A., Bernacchi, C. J., Davey, P. A., Ceulemans, R., & Scarascia-Mugnozza, G. E. (2005). Net carbon storage in a poplar plantation (POPFACE) after three years of free-air $CO_2$ enrichment. *Tree Physiology*, *25*, 1399–1408.

Harris, I., Jones, P. D., Osborn, T. J., & Lister, D. H. (2014). Updated high-resolution grids of monthly climatic observations—The CRU TS3.10 dataset. *International Journal of Climatology*, *34*, 623–642.

Hättenschwiler, S., & Körner, C. (1998). Biomass allocation and canopy development in spruce model ecosystems under elevated $CO_2$ and increased N deposition. *Oecologia*, *113*, 104–114.

Higgins, P. A. T., Jackson, R. B., Des Rosiers, J. M., & Field, C. B. (2002). Root production and demography in a California annual grassland under elevated atmospheric carbon dioxide. *Global Change Biology*, *8*, 841–850.

Hoosbeek, M. R., Lukac, M., Velthorst, E., Smith, A. R., & Godbold, D. L. (2011). Free atmospheric $CO_2$ enrichment increased above ground biomass but did not affect symbiotic $N_2$-fixation and soil carbon dynamics in a mixed deciduous stand in Wales. *Biogeosciences*, *8*, 353–364.

Hungate, B. A., Dijkstra, P., Wu, Z., Duval, B. D., Day, F. P., Johnson, D. W., Megonigal, J. P., Brown, A. L. P., & Garland, J. L. (2013). Cumulative response of ecosystem carbon and nitrogen stocks to chronic $CO_2$ exposure in a subtropical oak woodland. *The New Phytologist*, *200*, 753–766.

Hungate, B. A., Holland, E. A., Jackson, R. B., Chapin, F. S., III, Mooney, H. A., & Field, C. B. (1997). The fate of carbon in grasslands under carbon dioxide enrichment. *Nature*, *388*, 576–579.

Janssens, I. A., Medlyn, B., Gielen, B., Laureysens, I., Jach, M. E., van Hove, D., & Ceulemans, R. (2005). Carbon budget of *Pinus sylvestris* saplings after four years of exposure to elevated atmospheric carbon dioxide concentration. *Tree Physiology*, *25*, 325–337.

Jarvis, A., Reuter, H., Nelson, A., & Guevara, E. (2008). *Hole-filled SRTM for the globe Version 4*. http://srtm.csi.cgiar.org

Johnson, D. W., Hoylman, A. M., Ball, J. T., & Walker, R. F. (2006). Ponderosa pine responses to elevated $CO_2$ and nitrogen fertilization. *Biogeochemistry*, *77*, 157–175.

Kobayashi, S., Ota, Y., Harada, Y., Ebita, A., Moriya, M., Onoda, H., Onogi, K., Kamahori, H., Kobayashi, C., Endo, H., Miyaoka, K., & Takahashi, K. (2015). The JRA-55 reanalysis: General specifications and basic characteristics. *Journal of the Meteorological Society of Japan Series II*, *93*(1), 5–48.

Liberloo, M., Calfapietra, C., Lukac, M., Godbold, D., Luo, Z. B., Polle, A., Hoosbeek, M. R., Kull, O., Marek, M., Raines, C., & Rubino, M. (2006). Woody biomass production during the second rotation of a bio-energy *Populus* plantation increases in a future high $CO_2$ world. *Global Change Biology*, *12*, 1094–1106.

Mikan, C. J., Zak, D. R., Kubiske, M. E., & Pregitzer, K. S. (2000). Combined effects of atmospheric $CO_2$ and N availability on the belowground carbon and nitrogen dynamics of aspen mesocosms. *Oecologia*, *124*, 432–445.

Niklacs, P. A., Leadley, P. W., Schmid, B., & Körner, C. (2001). A long-term field study on biodiversity X elevated $CO_2$ interactions in grassland. *Ecological Monographs*, *71*, 341–356.

Olszyk, D. M., Johnson, M. G., Tingey, D. T., Rygiewicz, P. T., Wise, C., VanEss, E., Benson, A., Storm, M. J., & King, R. (2003). Whole-seedling biomass allocation, leaf area, and tissue chemistry for Douglas-fir exposed to elevated $CO_2$ and temperature for 4 years. *Canadian Journal of Forest Research*, *33*, 269–278.

Reich, P. B., & Hobbie, S. E. (2013). Decade-long soil nitrogen constraint on the $CO_2$ fertilization of plant biomass. *Nature Climate Change*, *3*, 278–282.

Riikonen, J., Lindsberg, M. M., Holopainen, T., Oksanen, E., Lappi, J., Peltonen, P., & Vapaavuori, E. (2004). Silver birch and climate change: Variable growth and carbon allocation responses to elevated concentrations of carbon dioxide and ozone. *Tree Physiology*, *24*, 1227–1237.

Schäppi, B., & Körner, C. (1996). Growth responses of an alpine grassland to elevated $CO_2$. *Oecologia*, *105*, 43–52.

Sheffield, J., Goteti, G., & Wood, E. F. (2006). Development of a 50-year high- resolution global dataset of meteorological forcings for land surface modeling. *Journal of Climate*, *19*, 3088–3111.

Smith, A. R., Lukac, M., Bambrick, M., Miglietta, F., & Godbold, D. L. (2013). Tree species diversity interacts with elevated $CO_2$ to induce a greater root system response. *Global Change Biology*, *19*, 217–228.

Spinnler, D., Egli, P., & Körner, C. (2002). Four-year growth dynamics of beech-spruce model ecosystems under $CO_2$ enrichment on two different forest soils. *Trees*, *16*, 423–436.

Stocker, B. D., Wang, H., Smith, N. G., Harrison, S. P., Keenan, T. F., Sandoval, D., Davis, T., & Prentice, I. C. (2020). P-model v1.0: An optimality-based light use efficiency model for simulating ecosystem gross primary production. *Geoscientific Model Development*, *13*(3), 1545–1581.

Talhelm, A. F., Pregitzer, K. S., Kubiske, M. E., Zak, D. R., Campany, C. E., Burton, A. J., Dickson, R. E., Hendrey, G. R., Isebrands, J. G., Lewin, K. F., Nagy, J., & Karnosky, D. F. (2014). Elevated carbon dioxide and ozone alter productivity and ecosystem carbon content in northern temperate forests. *Global Change Biology*, *20*, 2492–2504.

University of East Anglia Climatic Research Unit. (2019). *CRU JRA v2.0: A forcings dataset of gridded land surface blend of Climatic Research Unit (CRU) and Japanese Reanalysis (JRA) data*. Centre for Environmental Data Analysis.

Wang, H., Prentice, I. C., Keenan, T. F., Davis, T. W., Wright, I. J., Cornwell, W. K., Evans, B. J., & Peng, C. (2017). Towards a universal model for carbon dioxide uptake by plants. *Nature Plants*, *3*(9), 734–741.

Zak, D. R., Pregitzer, K. S., Curtis, P. S., Teeri, J. A., Fogel, R., & Randlett, D. L. (1993). Elevated atmospheric $CO_2$ and feedback between carbon and nitrogen cycles. *Plant and Soil*, *151*, 105–117.

Zhu, K., Chiariello, N. R., Tobeck, T., Fukami, T., & Field, C. B. (2016). Nonlinear, interacting responses to climate limit grassland production under global change. *Proceedings of the National Academy of Sciences of the United States of America*, *113*, 10589–10594.

Zhu, Z., Bi, J., Pan, Y., Ganguly, S., Anav, A., Xu, L., Samanta, A., Piao, S., Nemani, R., & Myneni, R. (2013). Global data sets of vegetation leaf area index (LAI)3g and fraction of photosynthetically active radiation (FPAR)3g derived from global inventory modeling and mapping studies (GIMMS) normalized difference vegetation index (NDVI3g) for the period 1981 to 2011. *Remote Sensing*, *2*, 927–948.

## SUPPORTING INFORMATION

Additional supporting information can be found online in the Supporting Information section at the end of this article.

**How to cite this article:** He, Y., Liu, Y., Lei, L., Terrer, C., Huntingford, C., Peñuelas, J., Xu, H., & Piao, S. (2023). $CO_2$ fertilization contributed more than half of the observed forest biomass increase in northern extra-tropical land. *Global Change Biology*, *29*, 4313–4326. https://doi.org/10.1111/gcb.16806